Photoinduced fluorescence intensity oscillation in a reaction-diffusion cell containing a colloidal quantum dot dispersion

Atsushi Komoto[a)]
Department of Chemical System Engineering, School of Engineering, The University of Tokyo, 7-3-1 Hongo, Bunkyo-ku, Tokyo 113-8656, Japan

Shinya Maenosono
School of Materials Science, Japan Advanced Institute of Science and Technology, 1-1 Asahidai, Nomi, Ishikawa, 923-1292, Japan

(Received 13 March 2006; accepted 27 July 2006; published online 19 September 2006)

The nonlinear spontaneous oscillation of photoluminescence (PL) intensity in an ensemble of semiconductor quantum dots (QDs), which differs from the fluorescence intermittency of a single QD, is investigated. The PL intensity in a QD dispersion slowly oscillates with time under continuous illumination. The oscillatory behavior is found to vary with changing QD concentration, solvent viscosity, volume fraction of irradiated region, and irradiation intensity. On the basis of the Gray-Scott model [*Chemical Oscillation and Instabilities: Non-linear Chemical Kinetics* (Clarendon, Oxford, 1994); J. Phys. Chem. **89**, 22 (1985); Chem. Eng. Sci. **42**, 307 (1987)], and its comparison with the experimental results, it is revealed that the following processes are important for PL oscillation: (1) mass transfer of QDs between the illuminated and dark regions, (2) autocatalytic formation of vacant sites on QD surfaces via photodesorption of ligand molecules, and (3) passivation of vacant sites via photoadsorption of water molecules. © *2006 American Institute of Physics*. [DOI: 10.1063/1.2338804]

I. INTRODUCTION

Colloidal semiconductor quantum dots (QDs) have attracted much attention because of their interesting optical properties, i.e., the quantum confinement effect.[1,2] The photophysical and electronic properties of QDs have been exposed by longstanding intensive studies,[3–7] and various optoelectronic devices, such as lasers,[3] light-emitting diodes,[4] and photovoltaic cells,[5] have been made as a result. QDs have also been used as luminescent labels for biological substances.[8,9] One of the striking characteristics of QDs is the fluorescence intermittency observed when a single QD is continuously excited, which is more commonly known as a "blinking" phenomenon.[6,7,10] The fluorescence intermittency has been found to be sensitive to environmental conditions. For example, the fluorescence "on" probability is dramatically enhanced when a QD is exposed to air immediately after being under vacuum conditions.[10] It means that the steady-state photoluminescence (PL) intensity of a QD ensemble is particularly sensitive to chemical species existing around the QDs. Based on this sensitivity, and the ease with which QDs can be surface functionalized, QDs are also expected to behave as good molecular sensors.[11–13]

We have recently reported the nonlinear spontaneous oscillation of the PL intensity of QDs, which is different from the fluorescence intermittency of a single QD.[14,15] The PL intensity of a QD ensemble (colloidal dispersion of QDs) slowly oscillates with time under continuous illumination. The PL oscillation behavior is also sensitive to the environment, such as *p*H (Ref. 14) and temperature,[15] and responds to the surroundings nonlinearly. In general, living organisms generate a nonlinear response to environmental conditions, while many artificial sensors are designed to produce a linear response. Thus, living things can gain much finer and more complicated information from the environment than artificial sensors. Therefore, it is expected that the PL oscillation is applicable to a nonlinear-response sensor, such that by functionalizing the QD surface, it becomes possible to analyze the change in oscillatory behavior with respect to different analytes and environmental conditions. In order to realize the potential of a nonlinear-response sensor based on PL oscillation, it is first necessary to clarify the mechanisms involved.

We have already found that PL oscillation is observed only over the course of QD aggregation.[15] Hence, it was inferred that the coverage dynamics of the functionalizing ligand is responsible for the PL oscillation. In this paper, we propose a theoretical model and compare the observed results with the obtained experimental results to reveal the underlying physics of the PL oscillation in a QD dispersion.

II. EXPERIMENTAL AND ANALYTICAL PROCEDURES

A. Materials

Tri-*n*-octylphosphine oxide (TOPO) (99% purity), tri-*n*-octylphosphine (TOP) (90% purity), and hexane (99% purity) were purchased from Aldrich, while *n*-tetradecanephosphonic acid (TDPA) (98% purity) was purchased from Avocado Research Chemicals. Dimethylcadmium ($CdMe_2$) (97% purity, 10 wt % in hexane) and sele-

[a)]FAX: (+81)-3-5841-7309. Electronic mail: komoto@chemsys.t.u-tokyo.ac.jp

nium (Se) powder (99.99% purity) were purchased from Strem Chemicals. Tetradecane (99.0% purity) and tri-*n*-butylphosphine (TBP) (98.0% purity) were purchased from Kanto Kagaku. Diethyldithiocarbamic acid zinc salt ($Zn[S_2CNEt]_2$) 99% purity) was purchased from Tokyo Kasei Kogyo. Toluene (99.5% purity), heptane (99.0% purity), octane (98.0% purity), nonane (98.0% purity), decane (99.0% purity), undecane (99.0% purity), dodecane (99.0% purity), tridecane (99.0% purity), pentadecane (97.0% purity), 1-octanol (98.0% purity), and 1-butanol (99.0% purity, dehydrated) were purchased from Wako Pure Chemical Industries.

B. Synthesis of CdSe/ZnS core/shell nanocrystals

CdSe core QDs were synthesized according to a previously published procedure that utilizes $CdMe_2$ as a cadmium source.[16] TOPO (2.931 g) and TDPA (0.069 g) were placed into a flask and heated up to 360 °C under an Ar atmosphere. Then, 2.0 ml of $CdMe_2$/Se/TBP mixture (molar ratio, Cd:Se:TBP=1.2:1.0:16.8) was rapidly injected into the hot-melted TOPO/TDPA matrix to form CdSe QDs capped with TOPO molecules. After injection of the $CdMe_2$/Se/TBP solution, the reaction temperature was maintained at 300 °C and CdSe QDs were allowed to grow for 10 min. Monodisperse CdSe QDs were separated from the matrix by antisolvent precipitation and decantation. The average diameter of the synthesized CdSe core QDs is ca. 2.6 nm, as estimated from the absorption peak (525 nm).[17]

Two monolayers of ZnS shells were subsequently grown on the CdSe cores using $Zn[S_2CNEt]_2$ as single-molecule precursors.[18] TOPO (3.00 g) and TOPO-capped CdSe QDs (0.080 g) were placed into a flask and heated up to 230 °C under an Ar atmosphere. A TOP solution of $Zn[S_2CNEt]_2$ (1.675 g, 10.0 wt %) was injected into the mixture, and the reaction temperature was maintained at 230 °C for 120 min. Then, 5.0 ml of 1-butanol was added to the flask. Monodisperse CdSe/ZnS core/shell QDs capped with TOPO molecules were separated from the matrix by antisolvent precipitation and decantation. The synthesized QDs were dried under vacuum and then stored in a vacuum desiccator. The average diameter of the CdSe/ZnS QDs was estimated to be ca. 4.2 nm, by taking into account the bulk lattice parameter of ZnS.[19]

C. PL measurement

CdSe/ZnS core/shell QDs were dissolved in various alkanes, toluene, and 1-octanol. A 2.0 ml portion of the QD dispersion was poured into a 10×10 mm^2 square quartz cuvette fitted with a screw cap. The concentration of the QD dispersions is varied from 5.0×10^{-4} to 0.20 mg/ml. The PL intensity was monitored at 540 nm using a fluorescence spectrophotometer (FP-6300, Jasco) and was recorded every 0.5 s for a period of 7500 s under continuous irradiation with a 400 nm excitation light (intensity I_{exc}=10 mW/cm^2). If necessary, I_{exc} was attenuated using neutral density (ND) filters. Figure 1 shows a schematic illustration of the experimental setup. The volume of the irradiated part of the dispersion in a square cuvette is about 0.24 cm^3 (12 vol %) [Fig. 1(a)]. The PL intensity at the center of the dispersion was measured. For the complete irradiation experiment, a 20 μl portion of the QD dispersion was poured into a 2×10 mm^2 microquartz cuvette with a screw cap and the cuvette position was raised using a pedestal in the spectrophotometer [Fig. 1(b)]. The QD dispersion temperature was tuned to 15 °C, at which point clear period-1 PL oscillations were observed[15] using an air-cooled Peltier device (EHC–573T, Jasco). The measurement was started 10 min after the cuvette was placed in the spectrophotometer to allow the temperature to equilibrate.

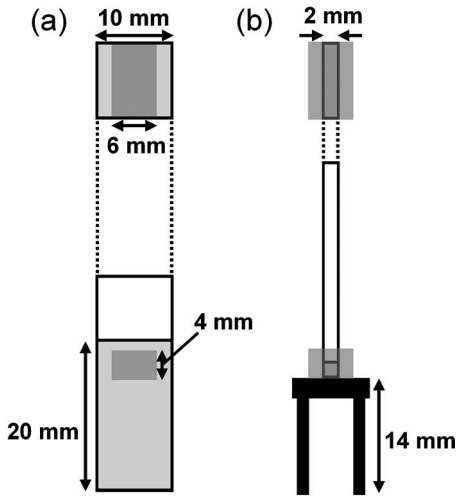

FIG. 1. Schematic illustrations of experimental setup. (a) Partial illumination and (b) complete illumination.

D. Analysis of time-series data

The time-series data of the PL intensity were analyzed by fast Fourier transform (FFT) to evaluate the frequency and power of the PL oscillation. The PL time-series data from 2500 to 7500 s were used for analysis, because the oscillatory behavior at the initial stage (<2500 s) is unsuitable for analysis. The data were normalized to the PL intensity at 2500 s and then the linear trend was removed. The normalized and trend-removed 5000 s data row $x(n)$ ($n=0,1,2,\ldots,N-1$; $N=10001$) was multiplied using a Hamming window $w(n)$ before FFT in order to avoid discontinuities at the beginning and end of a data set:

$$x_w(n) = x(n)w(n), \tag{1}$$

$$w(n) = 0.54 - 0.46\cos\left(\frac{2\pi n}{N-1}\right). \tag{2}$$

Magnitude spectrum $|X_w(k)|$ was obtained by computing FFT of $x_w(n)$:

$$X_w(k) = \sum_{n=0}^{N-1} x_w(n)\exp\left(-j\frac{2\pi}{N}kn\right), \quad k = 0,1,2,\ldots,N-1. \tag{3}$$

k is converted to frequency f,

$$f = \frac{k}{N} f_s, \tag{4}$$

where f_s is the sampling frequency (2 Hz). Although the magnitude spectra of the PL oscillation are broad, we defined the peak frequency in the spectrum as a representative value. The power of the oscillation P is calculated by

$$P = \sum_{n=0}^{N-1} |x_w(n)|^2 = \frac{1}{N} \sum_{n=0}^{N-1} |X_w(k)|^2 \quad \text{(Parseval's relation)}. \tag{5}$$

A short-time Fourier transform (STFT) was also applied to the time-series data for time-frequency analysis. In STFT, the 5000 s data were analyzed by FFT and the data region for FFT was moved every 500 s. The numerical simulation results of the mathematical model were also analyzed in the same manner and compared with the experimental results.

III. MODEL

The Gray-Scott model displays a wide range of patterns, such as temporal oscillations or multistabilities, although it consists of very simple differential equations.[20–22] In the typical Gray-Scott model, the following reactions are considered:

$$A + nB \xrightarrow{k_1} (n+1)B, \tag{6}$$

$$B \xrightarrow{k_2} C, \tag{7}$$

where k_1 and k_2 denote the reaction rate constants. The Gray-Scott model shows sustained oscillations in open systems.[20] In particular, two kinds of open system have been analyzed in the Gray-Scott model. The first is a continuously fed, well-stirred tank reactor[20,21] (CSTR) and the second is a reaction-diffusion cell.[20,22] In the CSTR model, reactants are fed from reservoirs and the products are delivered by flow. The Gray-Scott model in the case of CSTR is expressed by the following ordinary differential equations:

$$\frac{da}{dt} = k_f(a_0 - a) - k_1 a b^n, \tag{8}$$

$$\frac{db}{dt} = k_f(b_0 - b) + k_1 a b^n - k_2 b, \tag{9}$$

where a and b are the normalized concentrations of species A and B in the reactor, a_0 and b_0 are the normalized concentrations of species A and B in the reservoir, and k_f is the flow rate. The terms a and b are normalized to the total concentration of species used and fall within the range of 0–1. The first terms on the right-hand side in Eqs. (8) and (9) represent the flow of the species, while the remaining terms represent the chemical reactions corresponding to Eqs. (6) and (7).

In the case of a reaction-diffusion cell, the model is described by the following partial differential equations:

$$\frac{\partial a}{\partial t} = D\nabla^2 a - k_1 a b^n, \tag{10}$$

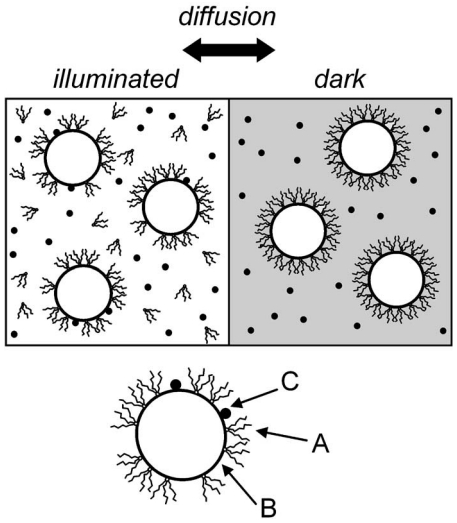

FIG. 2. Schematic illustration of the model for the PL oscillation. A, B, and C correspond to TOPO-adsorbed, vacant, and water-adsorbed sites, respectively.

$$\frac{\partial b}{\partial t} = D\nabla^2 b + k_1 a b^n - k_2 b, \tag{11}$$

where D is a diffusion coefficient. The space in the cell is divided into two zones: reaction and reservoir zones. Many qualitative similarities, such as the dependence of solutions on kinetic parameters, are found between the reaction-diffusion cell and the CSTR models.[20,22] Therefore, one can discuss the underlying physics qualitatively by using the CSTR model even in the case of a reaction-diffusion cell.

Here, we apply the Gray-Scott model to elucidate the PL oscillation phenomenon. The validity of the basis for applying the Gray-Scott model to the PL oscillation will be addressed in Sec. V in detail. We assume that A, B, and C correspond to the TOPO-adsorbed, vacant, and water-adsorbed sites, respectively. Equations (6) and (7) represent the photodesorption of TOPO molecules[15] and the photoadsorption of impurities, such as water molecules,[23,24] respectively. A partially illuminated QD dispersion in a cuvette is regarded as a reaction-diffusion cell, since both reactions [Eqs. (6) and (7)] are photoinduced processes and take place only in the illuminated region (Fig. 2). The illuminated and dark regions correspond to the reaction and reservoir zones in the reaction-diffusion cell model, respectively. However, for simplicity, we focus only on the region where the oscillation takes place and use the CSTR model instead of the reaction-diffusion model. Applying the CSTR model to our case assumes that the oscillatory region is spatially homogeneous. This simplified model is sufficient for the purposes of this paper, because the CSTR model is qualitatively equivalent to the reaction-diffusion cell model,[20,22] and because we focus only on the temporal pattern of the system.

The flow of species corresponds to the diffusion of QDs between the reaction and reservoir zones. In the reaction zone, the dangling bonds (vacant sites) on the QD surfaces are formed by irradiation. As such, the low-TOPO-coverage QDs diffuse from the reaction zone to the reservoir zone,

TABLE I. Standard kinetic parameters used in numerical simulations.

Parameter	Value
k_f (s^{-1})	0.035
k_1 (s^{-1})	14
k_2 (s^{-1})	0.7
r (−)	0.1

while the high-TOPO-coverage QDs diffuse in the reverse manner. Based on the above considerations, we modified Eqs. (8) and (9) as follows:

$$\frac{da}{dt} = k_f(a_0 - a) - k_1 ab, \tag{12}$$

$$\frac{db}{dt} = k_f(b_0 - b) + k_1 ab - \frac{k_2 b}{r + b}, \tag{13}$$

assuming $n=1$ in Eqs. (6) and (7). The kinetic rate of Eq. (7) is changed from $k_2 b$ to the Michaelis-Menten (MM) function $k_2 b/(r+b)$.[21] The MM-type reaction formulation arises if, for instance, the conversion from B to C proceeds on the surface.[21] In our case, Eq. (7) corresponds to the adsorption of water molecules onto the surface of the QDs, in which the rate is suppressed by increasing b, as mentioned in Sec. V.

To simplify the model, the following assumptions are introduced: (1) TOPO desorption and water adsorption are irreversible reactions; (2) the water concentration in the bulk phase is constant, since its concentration is much higher than a and b, as discussed later; (3) the coverage distribution from QD to QD is not considered; (4) the decrease in the diffusion coefficient of the QDs due to aggregation is not considered, i.e., k_f=const, because the size of the aggregates is only two to three times larger than that of a single QD at a maximum;[15] and (5) the concentrations of all species in the reservoir zone are constant, because the volume of the reservoir zone is seven times larger than that of the reaction zone (see below in the text).

The adsorption sites on the QD surfaces are thought to be completely occupied by TOPO molecules before irradiation, i.e., $(a,b)=(1,0)$. Based on assumption 5, $a_0=1$ and $b_0=0$, where $(a,b)=(1,0)$ represents one of the stationary solutions, meaning that no reactants are converted (zero conversion solution). The stability of this solution depends on the kinetic parameters, which become unstable when the other solution emerges.[21] As an initial condition, $(a,b)=(0.999,0.001)$ is chosen when taking the perturbation into account. Since the emission efficiency of the QDs depends mainly on the coverage of TOPO molecules, we use a in place of the PL intensity, assuming that the PL intensity is proportional to a. The standard values of the parameters used in the simulation are summarized in Table I.

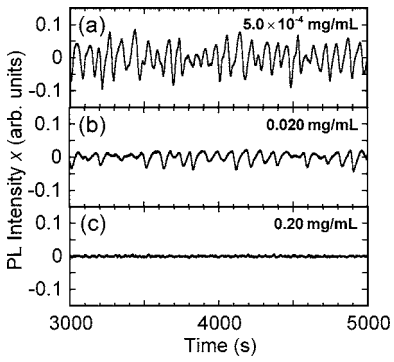

FIG. 3. Time evolutions of the PL intensity after normalization and removing linear trends in the QD/octane dispersions (η=0.58 mPa s and I_{exc}=10 mW/cm^2). The QD concentrations are (a) 5.0×10^{-4} mg/ml, (b) 0.020 mg/ml, and (c) 0.20 mg/ml.

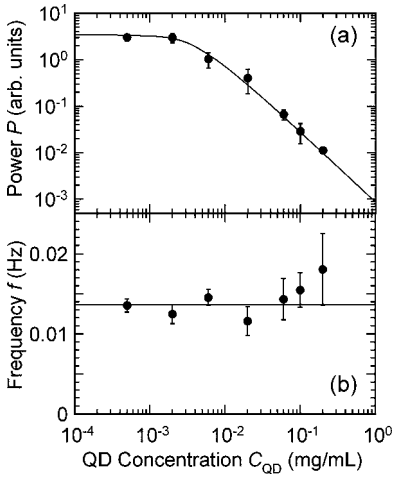

FIG. 4. QD concentration dependences of (a) P and (b) f in the case of QD/octane dispersion (η=0.58 mPa s and I_{exc}=10 mW/cm^2). The solid lines are drawn as guides.

IV. RESULTS

A. QD concentration

Figures 3 and 4 show the concentration dependence of the PL oscillation in a QD/octane dispersion. In Fig. 3, the time-series data of the PL intensity after removing the linear trend are shown. Before removing the linear trend, the PL intensity gradually decreases with oscillation under continuous irradiation. The power of the oscillation P increases with decreasing QD concentration C_{QD} as shown in Figs. 3 and 4(a). The PL oscillation was not clearly observed in the QD/octane dispersion in our previous study, because C_{QD} =0.19 mg/ml.[15] On the other hand, the oscillation frequency f is almost independent of C_{QD}, as shown in Fig. 4(b).

The PL intensity time-series data (5000 s) taken immediately after the initial 2500 s irradiation period were used for the Fourier analysis, and used defined the PL decay rate ΔI_{PL} (%) as

TABLE II. QD concentration dependence on PL decay rate.

	ΔI_{PL} (%)	
QD concentration (mg/ml)	Illuminated	Dark
5.0×10^{-4}	46.4±8.7	31.8±13.7
0.02	18.5±2.1	−1.1±1.1

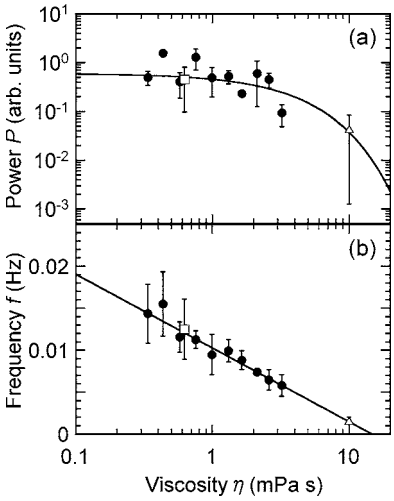

FIG. 5. Solvent viscosity dependences of (a) P and (b) f (C_{QD} =0.020 mg/ml and I_{exc}=10 mW/cm^2). The viscosity was varied by using a range of solvents. The filled circles, open squares, and open triangles represent the values in the QD/alkane, QD/toluene, and QD/1-octanol dispersions, respectively. The solid lines are drawn as guides.

$$\Delta I_{PL} = 100 \times \left(1 - \frac{I_{PL}^2}{I_{PL}^1}\right) \quad (\%), \tag{14}$$

where I_{PL}^1 and I_{PL}^2 are the PL intensities at 2500 and at 7500 s in the original time-series data, respectively, before removing the linear trend. As shown in Table II, the PL decay rate increases with decreasing QD concentration. This decay is presumably due to the desorption of TOPO molecules, determined according to our previous study.[15] Even in dark conditions, the PL intensity gradually decreases with time when $C_{QD}<0.020$ mg/ml. Since this gradual PL decay disturbs the analyses of the PL oscillation, the QD concentration is fixed at C_{QD}=0.020 mg/ml hereafter.

B. Solvent viscosity

The Belousov-Zhabotinsky (BZ) reaction is a well-known oscillatory system, whose behavior in a closed, unstirred system is known to be affected by both medium viscosity[25] and temperature.[26] We have previously confirmed that the temperature dependence of the PL oscillation is similar to that of the closed, unstirred BZ system.[15] The transition from periodic to chaotic oscillation through period doubling [Ruelle-Takens-Newhouse (RTN) scenario] was observed as the temperature increases. In the closed, unstirred BZ system, the chaotic attractor disappears with increasing medium viscosity (inverse RTN scenario).[25] Here, hydrodynamic effects such as convection are considered to be responsible for the inverse RTN scenario. Thus, we investigate the effect of solvent viscosity on the PL oscillation behavior. The viscosity was varied by using various alkane (C_6–C_{15}) solvents, since the viscosity of alkanes is known to increase with increasing chain length.[27–29] The solvent viscosity η at 15 °C is obtained by interpolating or extrapolating the value at each temperature reported in Refs. 27–29. Figure 5(a) shows the dependence of the PL oscillation power P on η, indicating that P is only marginally dependent on η when η <3 mPa s, while P appears to decrease with increasing η when $\eta>3$ mPa s. As shown in Fig. 5(b), the oscillation frequency f clearly decreases with increasing η. Note that the inverse RTN scenario is not observed in the PL oscillation, unlike in the closed unstirred BZ reaction.

It is possible that f is changed by some of the other physical properties associated with alkanes, namely, the dielectric constant, surface tension, or heat capacity. However, the f value of the QD/toluene dispersion is identical with that of the QD/alkane dispersion, whose viscosity is approximately the same as that of toluene [Fig. 5(b)]. Since the physical properties of toluene (except for viscosity) are vastly different from those of alkanes,[27] f is also considered to be determined by η in the QD/toluene dispersion. In addition, 1-octanol is used as a high-viscosity solvent to examine the viscosity dependence of f. As shown in Fig. 5(b), f in the case of the QD/1-octanol dispersion is much lower than in the cases of the QD/alkane dispersions, as determined from the viscosity-frequency master curve. Consequently, it is highly possible that η is one of a number of governing parameters for f.

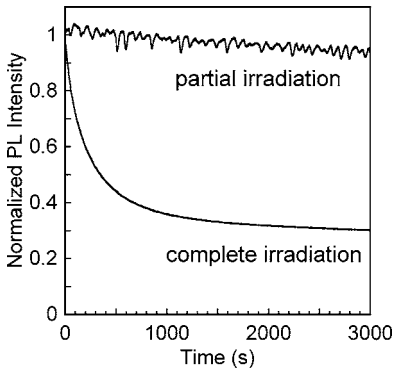

FIG. 6. Effect of the volume fraction of the irradiated region on temporal variation in the PL intensity (η=0.58 mPa s, C_{QD}=0.020 mg/ml, and I_{exc} =10 mW/cm^2). In the case of partial irradiation, the volume fraction of the irradiated regions is 12 vol %.

C. Volume fraction of irradiated region

To investigate the dependence of the oscillatory behavior on the volume fraction of the irradiated region, the QD/octane dispersion was completely irradiated by placing it in a microcuvette and reducing the dispersion volume [see Fig. 1(b)]. The PL oscillation is fully diminished when the dispersion is completely irradiated (Fig. 6). Additionally, the PL oscillation was fully diminished also when the dispersion was stirred vigorously (data not shown). These results indicate that the PL oscillation requires mass transfer processes between the illuminated and dark regions. As shown in Fig. 6, the PL intensity decays rapidly soon after irradiation begins under complete illumination, but decays slowly under partial illumination. This rapid PL decay is similar to the statistical aging, which is due to the nonergodicity of the blinking statistics of the QDs and observed in dispersed-QD films.[30,31] Here, however, the PL intensity did not recover when the dispersion was kept in the dark after illumination, unlike in the case of statistical aging.[31] Therefore, statistical aging can be ruled out as an origin of the rapid PL decay. On the other hand, the PL decay rate decreases as the volume

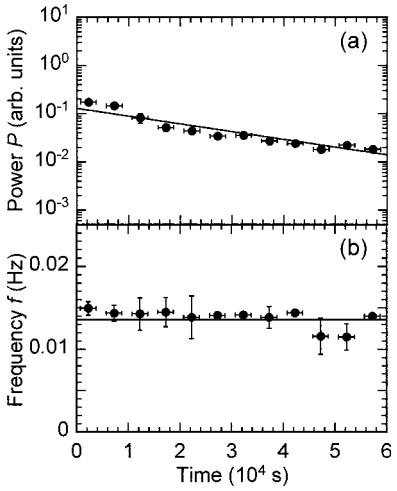

FIG. 7. Transient behavior of (a) P and (b) f (η=0.58 mPa s, C_{QD} =0.020 mg/ml, and I_{exc}=10 mW/cm^2). The solid lines are drawn as guides.

fraction of the dark part is increased. Thus, the enhancement of the PL decay rate in the case of complete illumination is possibly due to the lack of diffusion of fresh (nonilluminated, high-TOPO-coverage) QDs from the dark to illuminated regions.

D. Transient behavior and irradiation intensity dependence of PL oscillation

The PL oscillation is a transient phenomenon because the QD dispersion is a closed system, as pointed out in our previous study.[15] Figures 7(a) and 7(b) show the transient behaviors of the oscillation power P and the frequency f, extracted by STFT analysis. During the long-term irradiation of the QD dispersion, P gradually decreases with time [Fig. 7(a)], while f does not change [Fig. 7(b)]. The gradual decay of P is consistent with the result in our previous study. This indicates that the system gradually approaches the equilibrium state with QD aggregation.

Figure 8 shows the time evolutions of PL intensity when the irradiation intensity I_{exc} is reduced. In Fig. 8(a), the extinction of the PL oscillation through the damped oscillation is observed when I_{exc}=0.27 mW/cm^2. As shown in Fig. 8(b), the amplitude of the PL oscillation drastically decreases when I_{exc}=0.11 mW/cm^2, as compared with Fig. 3(b) where the distinct oscillation is observed (I_{exc}=10 mW/cm^2).

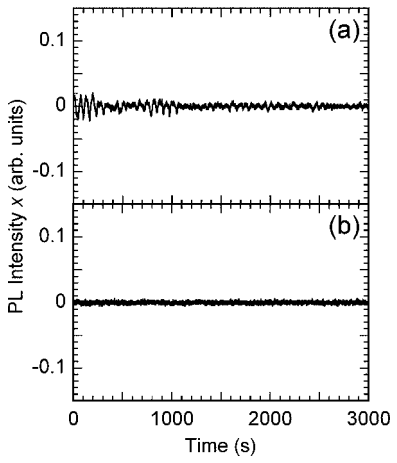

FIG. 8. Effect of irradiation intensity on the temporal variation of PL intensity (η=0.58 mPa s and C_{QD}=0.020 mg/ml): (a) I_{exc}=0.27 mW/cm^2 and (b) I_{exc}=0.11 mW/cm^2. A reduction in the irradiation intensity causes an apparent decrease in the magnitude of the oscillation, as compared with Fig. 3(b) (I_{exc}=10 mW/cm^2).

V. DISCUSSION

A. Physical meanings of the model

1. Autocatalytic reaction

Firstly, we discuss the validity of the basis for applying the Gray-Scott model to the PL oscillation. Our previous study indicated that TOPO molecules desorb from the QD surface under continuous excitation (photodesorption), where the photodesorption of TOPO molecules plays an important role in PL oscillation.[15] On the basis of previous reports, we attribute the origin of photodesorption to the photoionization of QDs in the course of the PL blinking. The blinking is caused by switching between the neutral (emissive, "on") and ionized (dark, "off") states of a QD.[7,30,32] The off period is produced by the ejection of excited electrons from a QD into neighboring trap sites, which exist either on the QD surface or in the surrounding materials.[7] In the QD dispersion, the neighboring solvent molecules are unable to trap electrons efficiently, since the electron affinity of organic solvents is much weaker than that of metal compounds.[27,33] Thus, the ejected electrons are considered to be mostly trapped by defects on the QD surfaces. Even if the electrons are transferred to a solvent molecule or other solute molecules, e.g., free TOPO molecules, water molecules, or other impurities, an electrostatic attraction between the positively charged QD core and the negatively charged (electron-captured) molecule is presumed to arrest charge separation. This is because the electrostatic energy between the positively charged QD and an electron located 5 nm away from the QD center is calculated to be 146 meV, which is six times larger than kT (25 meV at 15 °C). Hence, most electrons ejected from the QD cores are thought to exist on the QD surface, and thus, the electrostatic potential near the photoionized QD surface is estimated to be predominantly negative.[34] Since the coordinating site of the TOPO molecules (oxygen atom) is negatively polarized, the photoionization of the QDs destabilizes the adsorption of TOPO molecules. A first-principles calculation also suggested that the adsorption of ligand molecules onto the polar facet of QDs is less stable than adsorption onto nonpolar facets because of the higher electron density at the polar facet.[35] Moreover, the solvent molecules around the photoionized QDs would be polarized, causing a reduction in the activation energy for TOPO molecule desorption, because the isolated TOPO molecules are more stable in a slightly polarized solvent than in a nonpolar solvent.[36,37] Hence, desorption of the TOPO molecules from even neutral QDs would be induced when QDs form colloids with photoionized QDs.

On the other hand, the probability of off time occurring increases with decreasing TOPO coverage, since trap sites (i.e., vacant sites) at the QD surface are formed. As in similar cases, a longer off time is observed under vacuum, because

the QD surfaces are not passivated by water or oxygen molecules,[10] and the ZnS coating on the CdSe QDs increases the probability of an on state occurring.[6] As a consequence, since the photodesorption of TOPO molecules and the photoionization of QDs mutually accelerate the other process, the vacant sites are considered to be formed quasiautocatalytically. The rapid photoionization rate is 10^5-10^8 s^{-1},[7] and the QD collision rate is calculated to be <ca. 5000 s^{-1} using the Smoluchowski theory.[38] The time scale of these processes, which are considered to be responsible for the photodesorption of the TOPO molecules, is much smaller than the period of PL oscillation (<ca. 50 s). Thus, it is considered that QD blinking reaches preequilibrium with respect to TOPO desorption, and then some fraction of the excited QDs is always considered to be in the photoionized state, accelerating the photodesorption of TOPO molecules. Since a fraction of the photoionized QDs are thought to be an increasing function of b, the autocatalytic rate k_1ab could be applied to the photodesorption of TOPO molecules.

2. Mass transfer process and feedback reaction

As mentioned in Sec. IV, our experiments suggested that the PL oscillation requires the nonilluminated region in the QD dispersion. In the case of partial irradiation, only 12 vol % of the dispersion was illuminated by the excitation light [see Fig. 1(a)]. The decrease in the total coverage of TOPO molecules due to the photodesorption process in the illuminated region is relaxed by diffusion of the QDs between the illuminated and dark regions (Fig. 2). Hence, these two regions in the dispersion can be considered as the reaction zone (illuminated part) and reservoir zone (dark part) in a reaction-diffusion cell, respectively. The diffusion of QDs between the reaction and reservoir zones is expressed as the first terms on the right-hand side of Eqs. (12) and (13).

The Gray-Scott model without Eq. (7) in the reaction-diffusion cell, however, does not show oscillatory behavior, although it does show multistability.[20,22] Equation (7) represents the deactivation of the catalysis of B, which corresponds to the passivation of the vacant sites by water molecules in our case, as discussed in the following. It is known that the photoadsorption of water molecules passivates the surface states of a QD under continuous excitation, resulting in the enhancement of the emission quantum yield.[23,24] This PL enhancement results from the decrease in the photoionization probability of a single QD.[10] To calculate the concentration of adsorption sites and to compare this value with that of water, it is necessary to determine the molecular weight of the QD and the number of adsorption sites per dot. Here, the adsorption site is defined as a site available for TOPO adsorption. The molecular weight of CdSe QDs can be calculated by assuming that the QD is a sphere, where the density of each QD is equal to that of the bulk crystal, and the QD surface is coated with ten TOPO molecules per nm^2.[39] The number of adsorbed TOPO molecules is estimated to be 542 per dot in the case of as-synthesized QDs. According to this, we calculate the molecular weight of CdSe/ZnS QDs by

$$M_{\mathrm{QD}} = \left[\frac{4}{3}\pi r_{\mathrm{CdSe}}^3 d_{\mathrm{CdSe}} + \frac{4}{3}\pi (r_{\mathrm{CdSe/ZnS}}^3 - r_{\mathrm{CdSe}}^3) d_{\mathrm{ZnS}} + 4\pi r_{\mathrm{CdSe/ZnS}}^2 \left(10 \frac{M_{\mathrm{TOPO}}}{N_A} \right) \right] N_A, \tag{15}$$

where d is the bulk density, r is the radius of QD, M is the molecular weight, and N_A is Avogadro's number. By using $d_{\mathrm{CdSe}}=5.81\times10^{-21}$ g/nm^3, $d_{\mathrm{ZnS}}=4.10\times10^{-21}$ g/nm^3, $r_{\mathrm{CdSe/ZnS}}=2.1$ nm, $r_{\mathrm{CdSe}}=1.3$ nm, and $M_{\mathrm{TOPO}}=386.68$, we obtain $M_{\mathrm{QD}}=3.1\times10^5$. From these values, the concentration of adsorption sites is calculated to range from 0.87 μM ($C_{\mathrm{QD}}=5.0\times10^{-4}$ mg/ml) to 350 μM ($C_{\mathrm{QD}}=0.20$ mg/ml) in our experiments. On the other hand, the concentration of water in the octane used in the experiments was measured to be 30.3 ppm (1.18 mM), using a Karl Fisher coulometer (Metrohm). This value is much greater than the concentration of adsorption sites, i.e., total number of TOPO molecules. Therefore, once vacant sites are formed, these are preferentially passivated by the water molecules rather than by free TOPO molecules. Although the mechanism by which the water molecules become photoadsorbed onto the QD surface is still unknown, it is considered that these molecules, as well as TOPO molecules, stabilize the QD surface by coordination through their respective oxygen atoms.[24] The coordination of water molecules becomes increasingly difficult with increasing b due to the electrostatic potential near the photoionized QD surface, as indicated in the discussion for TOPO molecules. That is, the rate constant k_2 would appear to decrease in Eq. (9). As a result, the water adsorption rate tends to saturation as b increases. Hence, we adopt the MM-type function for the water adsorption reaction, as described in Eq. (13).

B. Comparison with experiment

1. QD concentration

As described in Sec. IV, the oscillation power P increases with decreasing QD concentration C_{QD} [Figs. 3 and 4(a)]. Since the PL oscillation is based on the instability in the TOPO molecule adsorption onto the QDs, as mentioned above and in Ref. 15, the decrease in C_{QD} is thought to induce instability in the TOPO adsorption, as reported by Dollefeld *et al.*[40] In addition, the PL decay rate is larger in low-concentration dispersions than in high-concentration ones, as shown in Table II. According to the Smoluchowski theory,[38] the collision rate between desorbed TOPO molecules and the QDs decreases with decreasing C_{QD}. Since the TOPO readsorption rate is determined by the sticking probability and the collision rate, the readsorption rate decreases with C_{QD},[36] providing a suitable explanation for the instability of the adsorbed TOPO molecules when C_{QD} is low.

2. Solvent viscosity

The frequency of the PL oscillation, f, decreases with increasing solvent viscosity η (Fig. 5). Since k_f is related to the diffusion coefficient of the QD, D_{QD}, as mentioned above, k_f is inversely proportional to η. On the other hand, k_1 and k_2 are expected to be independent of η, since f is found to be independent of C_{QD}, which determines the diffusion

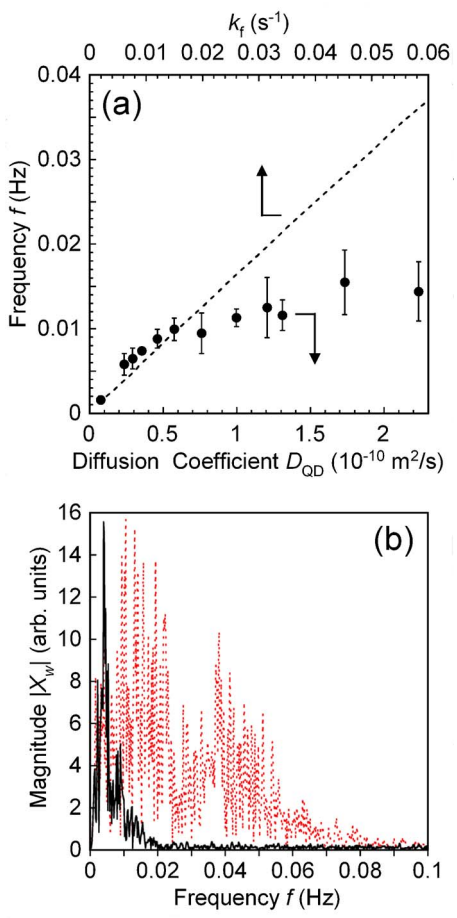

FIG. 9. (Color online) (a) Dependence of f on D_{QD}. The dashed line represents the calculated values of f, which is plotted vs k_f. (b) Magnitude spectra for QD/hexane (dotted line, $D_{QD}=1.3\times10^{-10}$) and QD/pentadecane (solid line, $D_{QD}=2.3\times10^{-11}$) dispersions.

length in the reactions on the QD surface [Fig. 4(b)]. In addition, we confirmed through theoretical means that the time constants in which the TOPO molecules, water molecules, and QDs diffuse between QDs are much larger than the PL oscillation period. Thus, we conclude that η only influences k_f, and compare the dependences of the oscillatory behavior on k_f in the model and D_{QD} in the experimental results.

Figure 9(a) shows f plotted versus D_{QD}. Assuming that the molecular length of TOPO is 0.7 nm, as reported in Ref. 41, and that the hydrodynamic diameter of the QD, d_{QD}, is 5.6 nm (QD diameter is 4.2 nm), D_{QD} is estimated by the Stokes-Einstein equation to be[38]

$$D_{QD}=\frac{k_BT}{3\pi\eta d_{QD}}, \tag{16}$$

where k_B is the Boltzmann constant and T is the temperature of dispersion. The dependence of f on k_f in the simulation is also shown in Fig. 9(a). The range of k_f is determined from the simulated curve fitting applied to the experimental values. As well as in the experimental results, f is also an increasing function of k_f in the simulation study. However, the value of f is found to be greater in the simulation study than in the experiments in the low-viscosity region ($D_{QD}>1.0\times10^{-10}$ m^2 s^{-1}, $k_f>0.026$ s^{-1}). This discrepancy is probably

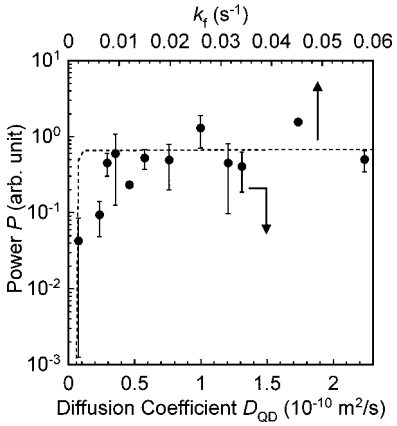

FIG. 10. Dependence of P on D_{QD}. The dashed line represents the calculated values of P, which is plotted vs k_f. The calculated values of P are reduced 300 times from their original values.

due to the intrinsic properties of the discrete-time Fourier transform (DFT), where FFT is one of the computational algorithms used in the DFT determination. Unlike in the idealized model, the actual PL oscillation contains various frequency components. The magnitude spectrum in the case of a low-viscosity (high-diffusivity) dispersion is calculated to be broader than in the case of a high-viscosity (low-diffusivity) dispersion, as shown in Fig. 9(b), since the frequency resolution increases with f in DFT. Additionally, the magnitude $|X_w|$ is overestimated by DFT as f decreases, resulting from convolution by window function (i.e., the Hamming window w in our case). Hence, f in the cases of the lower-viscosity dispersions is underestimated by our analysis. Since the steric repulsion between the QDs is reduced by photodesorption of the TOPO molecules, the QDs gradually aggregate during the course of PL oscillation.[15] Thus, k_f, i.e., D_{QD}, is likely to decrease with time. The term f, however, does not decrease over time [Fig. 7(b)]. It is believed that the aggregates formed under irradiation consist of only a few dots,[15] and thus D_{QD} is only slightly reduced via aggregation.

Figure 10 shows the dependences of P on D_{QD} and k_f. To compare the simulation study with the experimental results, the calculated values of P are reduced 300 times from their original values. This discrepancy between the calculated and experimental values of P will be discussed later. When $D_{QD}>2.5\times10^{-11}$ m^2 s^{-1} ($k_f>0.006$ s^{-1}), P does not depend on D_{QD} (k_f) both in the cases of the experimental and simulation results (Fig. 10). When $D_{QD}<2.5\times10^{-11}$ m^2 s^{-1} ($k_f<0.006$ s^{-1}), however, the experimental values of P decrease with decreasing D_{QD}, thus differing from the simulation results. The calculated values of P fall abruptly when $k_f\cong0.002$ s^{-1}. In the model, $k_f=0$ represents the system without a reservoir zone, corresponding to the case of the complete irradiation in Fig. 6. Thus, the decrease in D_{QD} converts the open system to a virtual closed system, decreasing P. In the actual system, there are many distributions, such as QD size and coverage distributions. Thus, the abrupt fall in P was not observed when $D_{QD}<2.5\times10^{-11}$, because the PL oscillation consists of various frequencies. Moreover, the experimental values of P would be underestimated at low D_{QD}, since it is difficult to differentiate the low-frequency components from the PL linear trend.

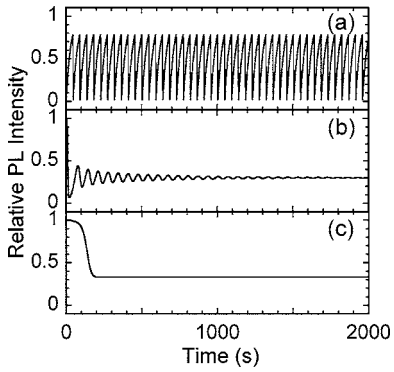

FIG. 11. Effect of irradiation intensity on the PL oscillation in the simulation: (a) $\kappa=1.0$, (b) $\kappa=0.065$, and (c) $\kappa=0.010$.

3. Irradiation intensity

Since Eqs. (6) and (7) are photoinduced processes in the PL oscillation, as mentioned above, the kinetic rate constants (k_1 and k_2) are considered to be increasing functions of I_{exc}. The dependence of k_1 and k_2 on I_{exc}, however, cannot be determined precisely. For simplicity, the values of k_1 and k_2 in the simulation were varied while keeping the ratio k_1/k_2 constant in order to examine the effect of I_{exc}. In the model, we define normalized kinetic constant κ, which corresponds to I_{exc}:

$$\kappa=\frac{k_1}{k_1^\circ}=\frac{k_2}{k_2^\circ}, \tag{17}$$

where $k_1^\circ=14\ \mathrm{s}^{-1}$ and $k_2^\circ=0.07\ \mathrm{s}^{-1}$ (i.e., the values of k_1 and k_2 when $I_{\mathrm{exc}}=10\ \mathrm{mW/cm}^2$; Table I). As shown in Figs. 11(a)–11(c), the Gray-Scott model predicts that the oscillatory behavior diminishes through damped oscillation as κ decreases. The transition from the sustained oscillation [Fig. 3(b)] to the stationary state [Fig. 8(b)] via damped oscillation [Fig. 8(a)] with decreasing I_{exc} is also observed in the experiment, indicating that the model prediction is proper.

In Figs. 12(a) and 13(a), the phase diagrams calculated by the model are shown. As shown in Fig. 12(a), there is a critical value of κ, κ_c, and the oscillation does not take place when κ is smaller than κ_c. κ_c decreases with decreasing k_f; that is, the model predicts that the oscillation can be observed in the case of high-viscosity dispersions even when I_{exc} is reduced. As shown in Fig. 13(a), f is found to be hardly dependent of I_{exc} and is expected to increase with k_f. To confirm these predictions, we made the phase diagrams corresponding to Figs. 12(b) and 13(b) from the experimental data (data points: 7×7) as shown in Figs. 12(b) and 13(b). The experimentally obtained phase diagrams [Figs. 12(b) and 13(b)] qualitatively agree with the theoretically predicted diagrams [Figs. 12(a) and 13(a)]. In the case of experiment, however, the region where the PL oscillation takes place is slightly larger than that in the case of theory. In short, the distinct boundary between the oscillatory and nonoscillatory regions cannot be seen in Fig. 12(b). This discrepancy is presumably because the transition region where the damped oscillation is observed is large in the case of experiment. As seen in Figs. 8(a) and 8(b), the PL oscillation was not diminished completely and small-amplitude oscillation was observed, even when I_{exc} was significantly decreased in the experimental system. Thus, f has a certain value even when I_{exc} is very low and P is quite small, as shown in Fig. 13(b). As mentioned above, the actual system contains various distributions, such as QD size and TOPO coverage, which are neglected in the model. Hence, the model could not reproduce the gradual transition from the oscillatory to the nonoscillatory state in the actual system. The emergence and the extinction of the PL oscillation are considered to be determined by the balance between the diffusion rate and the photoreaction rate in the reaction zone.

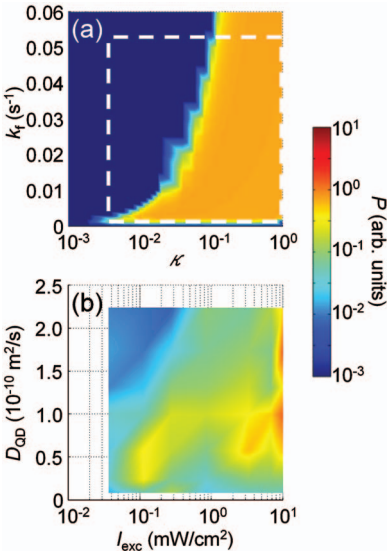

FIG. 12. (Color) Phase diagram of P with respect to QD diffusivity and irradiation intensity: (a) simulation and (b) experiment. The area surrounded by the dashed line in (a) corresponds to that in the experiment.

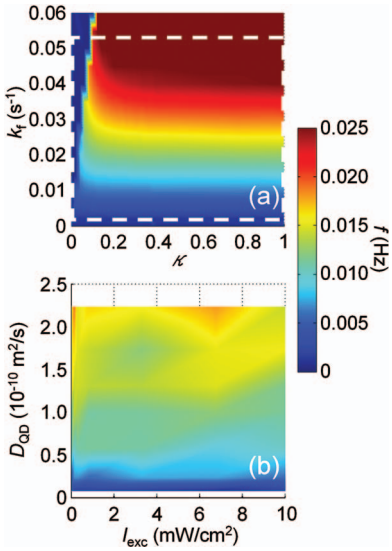

FIG. 13. (Color) Phase diagram of f with respect to QD diffusivity and irradiation intensity: (a) simulation and (b) experiment. The area surrounded by the dashed line in (a) corresponds to that in the experiment.

4. Evaluation

The emission quantum yield is assumed to be linearly proportional to a in the model, as mentioned above. The magnitude of the PL oscillation is determined to be a small

percentage of the average PL intensity in the experiment (Fig. 6), while the oscillation magnitude of a is a significant percentage of the average value of a in the simulation [Fig. 11(a)]. We infer that the smaller variation in the PL intensity in the experiment originates from the following: (1) The region which plays a role in the PL oscillation is expected to be of the order of a few percent of the total illuminated region. In the Gray-Scott model, the time scale of the flow rate in the CSTR model, k_f^{-1}, is equivalent to that of the diffusion in the reaction-diffusion model, $\tau_{\mathrm{diff}}=D_{\mathrm{QD}}/\delta^2$, where δ represents characteristic diffusion length.[20] Assuming that k_f^{-1} is equal to τ_{diff}, the characteristic diffusion length, $\delta=\sqrt{D_{\mathrm{QD}}/k_f}$, is estimated to be 62 μm, which is constant for all k_f values. This result implies that the PL oscillation takes place only near the boundary between the two zones, and the oscillating region is only a few percent of the total irradiated region. Actually, when we directly solve the reaction-diffusion cell model [Eqs. (10) and (11)] without simplification, the thickness of δ is less than 5% of the characteristic length of the illuminated spot. Hence, the k_f values are considered reasonable and proper. (2) The phase separation among QDs (low- and high-TOPO-coverage QDs) takes place due to readsorption of the TOPO molecules. It is highly likely that the TOPO molecules are selectively desorbed from certain QDs in order to stabilize other QDs. As a result, the QDs in the dispersion could be separated between TOPO-adsorption dominant QDs (ADQDs) and TOPO-desorption dominant QDs (DDQDs). In short, TOPO molecules desorbed from DDQDs could stabilize the ADQDs. The readsorption of TOPO molecules possibly reduces P when C_{QD} is higher [Fig. 4(a)], and the dispersion contains excess TOPO molecules.[15] Actually, the stationary state $(a,b)=(1,0)$ (no conversion solution) becomes stable and no oscillatory dynamics are observed when the rapid readsorption of TOPO molecules is considered in the model. In consequence, the ADQDs-DDQDs partition coefficient might be responsible for the power of the PL oscillation P.

Jones *et al.* reported that the observed time constant of the photoenhancement in a dissolved-methanol QD/hexane suspension is 5077 s in the case of $I_{\mathrm{exc}}\cong 70\ \mathrm{mW/cm^2}$.[24] They assumed that the photoenhancement is due to the photoadsorption of methanol molecules, which is thought to be same as that of water molecules. In this study, however, the time constant of the water photoadsorption is calculated to be $k_2^{-1}=1.43$ s in the case of $I_{\mathrm{exc}}=10\ \mathrm{mW/cm^2}$. Despite the lower illumination intensity, this value is much smaller than the observed value. k_2 is a function of dissolved-water concentration, because the model assumes that the water concentration is constant with respect to the variation of concentration of adsorption sites on QD surfaces. However, since the dissolved-methanol concentration is not specified in Ref. 24, we cannot compare the value used in the model with the observed value at the present time.

Previous studies on the Gray-Scott model revealed that a biperiodic oscillation emerges in the one-dimensional reaction-diffusion cell whose boundary conditions on the two sides are different.[42] Here, the volume of the dark region is finite and the dispersion is illuminated asymmetrically [Fig. 1(a)]. Therefore, the concentrations of each species near the interfaces between the irradiated and dark parts probably start to differ according to their location as the PL measurement proceeds. The boundary condition is assumed to be more complicated in our PL measurement than disclosed in the previous reports on the Gray-Scott model. Hence, the PL oscillation in the dispersion probably contains various frequency signals. In order to avoid the difficulty associated with the boundary conditions, the experimental setup should be changed from the reaction-diffusion cell to the CSTR. Then, the behaviors of the PL oscillation can be measured in the wide range of the parameters, e.g., the irradiation intensity and the flow rate. By comparing these experimental results with those obtained from the model, a wider and deeper understanding of the PL oscillation mechanism can be established.

VI. CONCLUSION

In a physical sense, the PL oscillation in the QD dispersion has some similarities with the Gray-Scott model in a reaction-diffusion cell. By applying the Gray-Scott model, the PL oscillation is considered to result from three processes: (1) the diffusion of QDs between the illuminated and dark regions in the dispersion, (2) the autocatalytic formation of the vacant sites due to the photoionization of QDs, and (3) the passivation of the vacant sites due to the photoadsorption of water molecules. The complex behaviors of the PL oscillation are suggested to be governed by the adsorption-desorption dynamics of the chemical species on the QD surfaces. In addition, we indicate the possibility that the ligand molecules (TOPO) adsorbed onto the QD surfaces are destabilized by the photoionization of QDs. To the best of our knowledge, this idea with respect to the photodesorption of ligands is new, and thus, provides new insights on the surface chemistry of the QDs, which is one of the most important issues for the QD research. Although there are several simplifications, the Gray-Scott model successfully reproduces important characteristics of the PL oscillation. In addition, the balance between the solvent viscosity (i.e., QD diffusivity) and the irradiation intensity (i.e., photoreaction rates) is found to play an important role in the PL oscillation. In the future, the oscillatory behaviors will be investigated in the wider range of the two parameters in order to understand the mechanism of the PL oscillation in detail.

ACKNOWLEDGMENTS

This work was supported by Research Fellowships of the Japan Society for the Promotion of Science for Young Scientists and the "Nanotechnology Materials Programs—Nanotechnology Particle Project" of the New Energy and Industrial Technology Development Organization (NEDO) based on funds provided by the Ministry of Economy, Trade and Industry, Japan (METI).

[1] A. P. Alivisatos, Science **271**, 933 (1996).
[2] C. J. Murphy, Anal. Chem. **74**, 520A (2002).
[3] M. Achermann, M. A. Petruska, S. Kos, D. L. Smith, D. D. Koleske, and V. I. Klimov, Nature (London) **429**, 642 (2004).
[4] S. Coe-Sullivan, J. S. Steckel, W. K. Woo, M. G. Bawendi, and V. Bulovic, Adv. Funct. Mater. **15**, 1117 (2005).

[5] I. Gur, N. A. Fromer, M. L. Geier, and A. P. Alivisatos, Science **310**, 462 (2005).
[6] M. Nirmal, B. O. Dabbousi, M. G. Bawendi, J. J. Macklin, J. K. Trautman, T. D. Harris, and L. E. Brus, Nature (London) **383**, 802 (1996).
[7] M. Kuno, D. P. Fromm, S. T. Johnson, A. Gallagher, and D. J. Nesbitt, Phys. Rev. B **67**, 125304 (2003).
[8] K. Hanaki, A. Momo, T. Oku, A. Komoto, S. Maenosono, Y. Yamaguchi, and K. Yamamoto, Biochem. Biophys. Res. Commun. **302**, 496 (2003).
[9] B. Dubertret, P. Skourides, D. J. Norris, V. Noireaux, A. H. Brivanlou, and A. Libchaber, Science **298**, 1759 (2002).
[10] J. Muller, J. M. Lupton, A. L. Rogach, J. Feldmann, D. V. Talapin, and H. Weller, Appl. Phys. Lett. **85**, 381 (2004).
[11] A. Y. Nazzal, L. H. Qu, X. G. Peng, and M. Xiao, Nano Lett. **3**, 819 (2003).
[12] X. J. Ji, J. Y. Zheng, J. M. Xu, V. K. Rastogi, T. C. Cheng, J. J. DeFrank, and R. M. Leblanc, J. Phys. Chem. B **109**, 3793 (2005).
[13] A. R. Clapp, I. L. Medintz, J. M. Mauro, B. R. Fisher, M. G. Bawendi, and H. Mattoussi, J. Am. Chem. Soc. **126**, 301 (2004).
[14] S. Maenosono, N. Eiha, and Y. Yamaguchi, J. Phys. Chem. B **107**, 2645 (2003).
[15] A. Komoto, S. Maenosono, and Y. Yamaguchi, Langmuir **20**, 8916 (2004).
[16] C. B. Murray, D. J. Norris, and M. G. Bawendi, J. Am. Chem. Soc. **115**, 8706 (1993).
[17] W. W. Yu, L. H. Qu, W. Z. Guo, and X. G. Peng, Chem. Mater. **15**, 2854 (2003).
[18] M. A. Malik, P. O'Brien, and N. Revaprasadu, Chem. Mater. **14**, 2004 (2002).
[19] B. O. Dabbousi, J. Rodriguez-Viejo, F. V. Mikulec, J. R. Heine, H. Mattoussi, R. Ober, K. F. Jensen, and M. G. Bawendi, J. Phys. Chem. B **101**, 9463 (1997).
[20] P. Gray and S. K. Scott, *Chemical Oscillations and Instabilities: Nonlinear Chemical Kinetics* (Clarendon, Oxford, 1994).
[21] P. Gray and S. K. Scott, J. Phys. Chem. **89**, 22 (1985).
[22] S. K. Scott, Chem. Eng. Sci. **42**, 307 (1987).
[23] S. R. Cordero, P. J. Carson, R. A. Estabrook, G. F. Strouse, and S. K. Buratto, J. Phys. Chem. B **104**, 12137 (2000).
[24] M. Jones, J. Nedeljkovic, R. J. Ellingson, A. J. Nozik, and G. Rumbles, J. Phys. Chem. B **107**, 11346 (2003).
[25] N. Marchettini and M. Rustici, Chem. Phys. Lett. **317**, 647 (2000).
[26] M. Masia, N. Marchettini, V. Zambrano, and M. Rustici, Chem. Phys. Lett. **341**, 285 (2001).
[27] D. R. Lide, *CRC Handbook of Chemistry and Physics: A Ready-reference Book of Chemical and Physical Data*, 83rd ed. (CRC, Boca Raton, FL, 2002).
[28] J. G. Wu, A. H. Nhaesi, and A. F. A. Asfour, Fluid Phase Equilib. **164**, 285 (1999).
[29] J. H. Dymond and H. A. Oye, J. Phys. Chem. Ref. Data **23**, 41 (1994).
[30] X. Brokmann, J. P. Hermier, G. Messin, P. Desbiolles, J. P. Bouchaud, and M. Dahan, Phys. Rev. Lett. **90**, 120601 (2003).
[31] I. H. Chung and M. G. Bawendi, Phys. Rev. B **70**, 165304 (2004).
[32] R. Verberk, J. W. M. Chon, M. Gu, and M. Orrit, Physica E (Amsterdam) **26**, 19 (2005).
[33] M. Meunier, N. Quirke, and D. Binesti, Mol. Simul. **23**, 109 (1999).
[34] S. Maenosono, Chem. Phys. Lett. **376**, 666 (2003).
[35] L. Manna, L. W. Wang, R. Cingolani, and A. P. Alivisatos, J. Phys. Chem. B **109**, 6183 (2005).
[36] P. W. Atkins, *Physical Chemistry*, 4th ed. (Oxford University Press, Oxford, 1990).
[37] K. Akiba, M. Wada, and T. Kanno, J. Inorg. Nucl. Chem. **42**, 261 (1980).
[38] W. B. Russel, D. A. Saville, and W. R. Schowalter, *Colloidal Dispersions* (Cambridge University Press, Cambridge, 1989).
[39] A. Striolo, J. Ward, J. M. Prausnitz, W. J. Parak, D. Zanchet, D. Gerion, D. Milliron, and A. P. Alivisatos, J. Phys. Chem. B **106**, 5500 (2002).
[40] H. Dollefeld, K. Hoppe, J. Kolny, K. Schilling, H. Weller, and A. Eychmuller, Phys. Chem. Chem. Phys. **4**, 4747 (2002).
[41] J. Jiang, T. D. Krauss, and L. E. Brus, J. Phys. Chem. B **104**, 11936 (2000).
[42] C. Kaaspetersen, J. Comput. Appl. Math. **26**, 187 (1989).